

Self-organized phase-locking of a mixed-resonant cavity diode laser array enabled by on-chip Talbot effect

Jun Qi(齐军), Tian Lan(兰天), Jing-Hao Zhang(张敬昊), Ying Li(李颖), Yi-Wen Lou(楼亦文), Feng-Jiao Qin(覃凤姣), Yu-Ying Liu(刘豫颖), and Zhi-Yong Wang(王智勇)

Citation: Chin. Phys. B, 2025, 34 (**7**): 074215. DOI: 10.1088/1674-1056/ade387
http://cpb.iphy.ac.cn; http://iopscience.iop.org/cpb

What follows is a list of articles you may be interested in

An adjustment-free laser resonator based on micron-scale corner cube array

Pengyuan Chang(常鹏媛), Xinrong Huang(黄欣荣), Caolei Fu(傅曹雷), Aiping Liu(刘爱萍), Duo Pan(潘多), Zhiyang Wang(王志洋), and Jingbiao Chen(陈景标)

Chin. Phys. B, 2025, 34 (**3**): 034201. DOI: 10.1088/1674-1056/ada434

High peak power mini-array quantum cascade lasers operating in pulsed mode

Yuhang Zhang(章宇航), Yupei Wang(王渝沛), Xiaoyue Luo(罗晓玥), Chenhao Qian(钱晨灏), Yang Cheng(程洋), Wu Zhao(赵武), Fangyuan Sun(孙方圆), Jun Wang(王俊), and Zheng-Ming Sun(孙正明)

Chin. Phys. B, 2025, 34 (**1**): 014204. DOI: 10.1088/1674-1056/ad886b

Tunable artificial plasmonic nanolaser with wide spectrum emission operating at room temperature

Peng Zhou(周鹏), Jia-Qi Guo(郭佳琦), Kun Liang(梁琨), Lei Jin(金磊), Xiong-Yu Liang(梁熊玉), Jun-Qiang Li(李俊强), Xu-Yan Deng(邓绪彦), Jian-Yu Qin(秦建宇), Jia-Sen Zhang(张家森), and Li Yu(于丽)

Chin. Phys. B, 2024, 33 (**5**): 054210. DOI: 10.1088/1674-1056/ad2dca

High-speed directly modulated distributed feedback laser based on detuned loading and photon-photon resonance effect

Yun-Shan Zhang(张云山), Yi-Fan Xu(徐逸帆), Ji-Lin Zheng(郑吉林), Lian-Yan Li(李连艳), Tao Fang(方涛), and Xiang-Fei Chen(陈向飞)

Chin. Phys. B, 2023, 32 (**9**): 094204. DOI: 10.1088/1674-1056/acc8c1

Geometrical condition for observing Talbot effect in plasmonics infinite metallic groove arrays

Afshari-Bavil Mehdi, Xiao-Ping Lou(娄小平), Ming-Li Dong(董明利), Chuan-Bo Li(李传波), Shuai Feng(冯帅), Parsa Saviz, Lian-Qing Zhu(祝连庆)

Chin. Phys. B, 2018, 27 (**12**): 124204. DOI: 10.1088/1674-1056/27/12/124204

Self-organized phase-locking of a mixed-resonant cavity diode laser array enabled by on-chip Talbot effect

Jun Qi(齐军)[1,2], Tian Lan(兰天)[1,2,†], Jing-Hao Zhang(张敬昊)[1,2], Ying Li(李颖)[3], Yi-Wen Lou(楼亦文)[1,2], Feng-Jiao Qin(覃凤姣)[1,2], Yu-Ying Liu(刘豫颖)[1,2], and Zhi-Yong Wang(王智勇)[1,2,‡]

[1] *Institute of Advanced Technology on Semiconductor Optics & Electronics, Physics and Optoelectronic Engineering, Beijing University of Technology, Beijing* 100124, *China*

[2] *Key Laboratory of Trans-scale Laser Manufacturing Technology (Beijing University of Technology), Ministry of Education, Beijing* 100124, *China*

[3] *Beijing Institute of Radio Metrology and Measurement, Beijing* 100124, *China*

(Received 27 March 2025; revised manuscript received 28 May 2025; accepted manuscript online 11 June 2025)

To address the challenge of achieving stable in-phase coherent optical field in high-power laser arrays, we propose a novel dual Talbot diffraction coupling method that combines the on-chip self-injection effect with a mixed-resonant cavity diode laser array (MDLA). The designed MDLA incorporates two types of resonant cavities and an integrated external fractional Talbot cavity to compensate for in-phase mode phase delays. Numerical simulations demonstrate that the near-field optical pattern can be self-imaged via self-organized phase-locking, while the far-field optical pattern of in-phase mode can be coherently enhanced and modulated to exhibit a single-lobe pattern successfully. Furthermore, this method could inherently provide strong optical coupling and overcome the limited scalability of the weakly-coupled laser arrays. Ultimately, by leveraging self-organized phase-locking and Talbot-induced mode discrimination, our approach offers a robust platform for realizing high-power coherent laser sources with scalable integration potential.

Keywords: mixed-resonant cavity, Talbot effect, self-injection effect, in-phase-locking

PACS: 42.55.Px, 42.55.Tv, 42.55.Ah, 85.30.–z

DOI: 10.1088/1674-1056/ade387 **CSTR:** 32038.14.CPB.ade387

1. Introduction

Diode laser arrays (DLAs), known for their monolithic integration, high efficiency, and scalable power output, have been attracting increasing attention in diverse application domains, such as laser pumping, laser processing, optical communication, laser defense, biomedical applications, and so on.[1–6] However, the inherent wide lateral dimension of each laser unit and low fill factor in conventional DLAs generally result in incoherent laser beams, and the far-field patterns (FFPs) exhibit multiple diffused lobes with no phase correlations, resulting in poor beam quality. Therefore, a complex and costly external beam shaping system is usually required to overcome this intrinsic beam quality limitation.[7–10]

Various methods have been explored to achieve highly integrated, high-beam-quality coherent DLAs, such as evanescent-wave coupling and X-junction coupling, but they often result in the out-of-phase mode.[11–15] Improved designs using Y-junction waveguides and anti-waveguides have been proven to enable in-phase operation.[16–20] However, these coupling methods struggle to maintain high coherence in large-scale DLAs due to their limited inter-coupling strength and high sensitivity to current and thermal fluctuations.

In recent years, phase-shifted DLAs and on-chip external Talbot cavity DLAs have been proposed as two types of innovative solutions to solve the above problems. The former one mainly involves phase compensation methods to suppress the out-of-phase mode. For instance, Zhou *et al.*[21] reported a photonic crystal DLA with a phase shift layer, which successfully converted the out-of-phase mode to the in-phase mode and reduced the lateral full width at half maximum (FWHM) divergence angle to 1.5° with a single-lobe FFP. The other approach relies on the Talbot effect, which has the advantage of being a parallel coupling approach with strong diffractive coupling, and it can also differentiate strongly between modes. For example, Liu's team[22–24] repeatedly reported quantum cascade laser (QCL) arrays based on the Talbot effect to realize in-phase mode output, such as an intracavity spatial filter QCL array, a tapered QCL array, and a terahertz QCL array. The lateral divergence angle was measured to be 1.5°, 2.7°, and 4°, respectively. In our previous work, we also introduced a monolithically integrated Fourier filter for phase-delay compensation, realizing controlled in-phase coupling.[25] Nevertheless, more strategies to accomplish phase delay compensation based on the fractional Talbot effect remain underexplored.

In this paper, we propose a specifically designed one-dimensional mixed-resonant cavity diode laser array (MDLA), incorporating two types of laterally interleaved resonant cav-

†Corresponding author. E-mail: lantian9094@bjut.edu.cn

‡Corresponding author. E-mail: zywang@bjut.edu.cn

© 2025 Chinese Physical Society and IOP Publishing Ltd. All rights, including for text and data mining, AI training, and similar technologies, are reserved.

ities, i.e., long-resonant cavities (LRCs), short-resonant cavities (SRCs), along with an integrated external cavity (EC). We subsequently illustrate a dual Talbot diffraction coupling mechanism, in which the EC employs fractional external Talbot cavity feedback to establish coherent phase locking between LRCs and SRCs. By engineering the effective index difference (EID) and resonant cavity length difference, the phase delay arising from the fractional Talbot effect is effectively compensated. The simulation results show that the coherence in the far field of the in-phase mode is enhanced. Ultimately, stable in-phase mode output is successfully established without external optical components, which allows the MDLA to be used in laser ranging.

2. Principle and design

2.1. Principle of MDLA

The initial optical field from the fundamental lateral mode of an infinite DLA can be expanded into a Fourier series[26]

$$E\left(x, z=0\right)=\sum A_m \exp\left(\mathrm{j}\frac{2\pi m x}{p}\right), \tag{1}$$

where $\mathrm{j}=\sqrt{-1}$, p is the period of a laser unit, and A_m is the complex weight of the Fourier component.

The free-space transfer function at one-quarter of the Talbot distance ($Z_\mathrm{t}/4=p^2/(2\lambda)$) is given by

$$\begin{aligned} H\left(m, z=\frac{Z_\mathrm{t}}{4}\right) &= \exp(\mathrm{j}kz)\exp\left(-\mathrm{j}\frac{\pi\lambda z m^2}{p^2}\right) \\ &= \exp(\mathrm{j}kz)\exp\left(-\mathrm{j}\frac{\pi m^2}{2}\right), \end{aligned} \tag{2}$$

where $k=2\pi/\lambda$ is the wave vector, $\exp(\mathrm{j}kz)$ is a constant phase term, and $\exp(-\mathrm{j}\pi m^2/2)$ is a phase delay term. When m is an even integer, the phase delay is 0. When m is an odd integer, the phase delay is $\pi/2$.

Ignoring the constant phase term again, the optical field at one-quarter of the Talbot distance is expressed as

$$\begin{aligned} E\left(x, z=\frac{Z_\mathrm{t}}{4}\right) &= \sum A_m \exp\left(\mathrm{j}\frac{2\pi m}{p}x\right)\exp\left(-\mathrm{j}\frac{\pi m^2}{2}\right) \\ &= \sum A_m \exp\left(\mathrm{j}\frac{2\pi m\left(x-pm/4\right)}{p}\right). \end{aligned} \tag{3}$$

In Eq. (3), within one period of the Talbot distance, m can take the values 0, 1, 2, 3, or 4, corresponding to five different optical field distributions. When $m=1$ or 3, the optical fields of the out-of-phase mode are shifted by $p/4$ and $3p/4$ perpendicular to the propagation direction, respectively. Here, we only analyze the in-phase mode optical fields corresponding to $m=0$, 2, and 4. When $m=0$ and 4, the in-phase mode optical fields are shifted by 0 and p, respectively, corresponding to a phase delay of 0 in Eq. (2). When $m=2$, the in-phase mode optical field is shifted by $p/2$, corresponding to the phase delay of $\pi/2$ in Eq. (2).[26]

Similarly, when $z=Z_\mathrm{t}/8$, in Eq. (3), when $m=0$, 2, 4, 6, and 8, the corresponding in-phase mode optical field positions are shifted by 0, $p/4$, $p/2$, $3p/4$, and p, respectively. Thus, the phase delay term of Eq. (2) becomes $\exp(-\mathrm{j}\pi m^2/4)$, and the phase delays corresponding to these five optical fields are 0, $\pi/4$, π, $\pi/4$, and 0, respectively, with three different phases.[27]

2.2. Design of MDLA

Based on the above analysis of in-phase mode optical fields at $Z_\mathrm{t}/4$ and $Z_\mathrm{t}/8$, the MDLA integrated with a fractional external Talbot cavity is designed to achieve in-phase locking, as shown in Fig. 1, consisting of two types of resonant cavities, i.e., LRC and SRC, and the integrated EC. In LRC, the $\mathrm{EC_l}$ length L is set to $Z_\mathrm{t}/8$, the corresponding round-trip cavity length is $Z_\mathrm{t}/4$. Thus, the out-of-phase mode optical fields are shifted by $p/4$ and $3p/4$, resulting in the optical injection into the non-gain region between LRC and SRC and then optical loss. Meanwhile, the in-phase optical field with zero phase-delay could completely propagate back into the LRC, while those with a phase delay of $\pi/2$ could then inject into the SRC. Subsequently, the difference ΔL between the cavity length of LRC and SRC is designed to be $Z_\mathrm{t}/4$ and then the corresponding $\mathrm{EC_s}$ length of SRC becomes $\Delta L+L=3Z_\mathrm{t}/8$. As a result, the optical round-trip in the $\mathrm{EC_s}$ length is set to $3Z_\mathrm{t}/4$, leading to the optical loss of out-of-phase mode in SRC and the self-injection of in-phase mode with zero phase delay and injection into the LRC with $-\pi/2$ phase-delay since[27]

$$\phi\left(Z_\mathrm{t}/4\right)=-\phi\left(3Z_\mathrm{t}/4\right). \tag{4}$$

In this way, self-organized in-phase phase-locking of the MDLA is achieved.

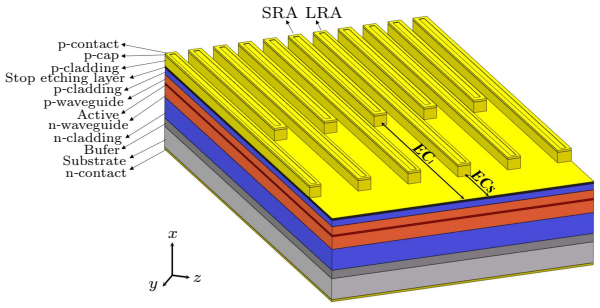


Fig. 1. Schematic of the proposed MDLA based on a typical 808 nm laser structure.

In order to achieve phase-locking of the in-phase mode, we calculated the relationship between the EID Δn and phase difference $\Delta\phi$ of MDLA with the etching depth h. It is hypothesized that the device structure is not limited to a specific substrate type and wavelength. For instance, the typical 808 nm laser epitaxial structure contains a 500 nm-thick

GaAs buffer layer on a GaAs substrate, followed by a 900 nm-thick layer, a thick $Al_{0.5}GaAs$ n-cladding layer, a 600 nm-thick $Al_{0.35}GaAs$ n-waveguide layer, the active layer contains a 7 nm-thick $GaAsP_{0.16}$ quantum well, and two 8 nm-thick $Al_{0.3}GaAs$ quantum barriers, a 400 nm-thick $Al_{0.35}GaAs$ p-waveguide layer and a 900 nm-thick $Al_{0.5}GaAs$ p-cladding layer. In order to achieve good ohmic contact between the electrode and the epitaxial material, a p-cap layer of 150 nm-thick GaAs is designed on top of the p-type cladding layer. The effective refractive index n_l of the 808 nm chip is 3.42420 originally. The etching depths of the MDLA are rationally designed to achieve phase compensation by

$$\Delta\phi = 2\pi \cdot \Delta n \cdot \Delta L/\lambda. \tag{5}$$

As shown in Fig. 2, when the etching depth is set to 0.74 μm, the effective refractive index n_s is calculated to be 3.42354. Consequently, the EID Δn between the LRC (SRC) and SRC (LRC) is 6.6×10^{-4} (-6.6×10^{-4}), thus leading to the phase difference $\Delta\phi$ of $\pi/2$ ($-\pi/2$). Based on the single-mode cut-off condition, the waveguide width is calculated, and it is found that when the ridge waveguide width w is less than 3.999 μm, only fundamental transverse mode exists. To precisely control the etching depth, we inserted a wet barrier layer with a thickness of 20 nm into the p-cladding layer.

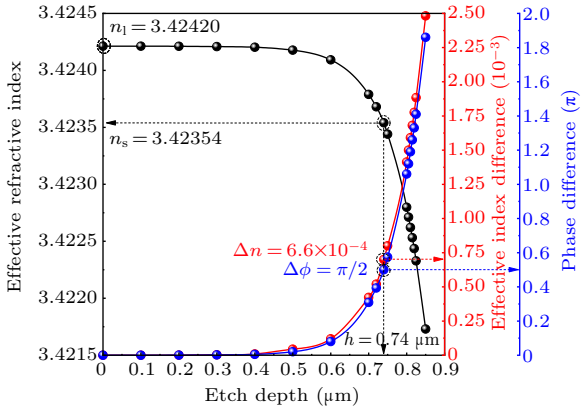


Fig. 2. The relationship between the EID and phase difference of MDLA with etching depth ranging from 0 to 0.85 μm.

3. Results of simulation and discussion

3.1. Talbot effect of DLA

In this study, the mechanism underlying the observed gain threshold differences between the in-phase mode and out-of-phase mode is further elucidated. It is well-established that both in-phase and out-of-phase mode optical fields are capable of achieving self-imaging at the Z_t ($Z_t = 2n_s p^2/\lambda$). However, in comparison to the out-of-phase mode, which can achieve self-imaging at a propagation distance $Z_t/2$, the in-phase mode optical field is entirely incapable of achieving self-imaging at any fractional Talbot distance. Consequently, the in-phase modes are unable to achieve effective self-injection, resulting in lower mode coupling strength and higher thresholds, which is the primary cause of the formation of supermode gain threshold differences.[28–30]

In accordance with the principles of coupled mode theory, the magnitude of the coupling strength of the supermode can be articulated as follows:

$$C_j = \frac{\int E_{j,\mathrm{tol}}(x,0)\, E^*_{j,\mathrm{tol}}(x,z)\,\mathrm{d}x}{\int E_{j,\mathrm{tol}}(x,0)\, E^*_{j,\mathrm{tol}}(x,0)\,\mathrm{d}x}, \tag{6}$$

where j is the jth order supermode, $E_{j,\mathrm{tol}}(x,0)$ is the initial optical field of the jth order supermode, $E^{j,*}_{\mathrm{tol}}(x,0)$ is the conjugate optical field of $E_{j,\mathrm{tol}}(x,0)$, and $E^{j,*}_{\mathrm{tol}}(x,z)$ is the conjugate optical field of the jth order supermode propagation over a distance z.

The integrated external cavity DLA can be equated to a composite cavity, and the effective reflectivity can be expressed as

$$R_{\mathrm{eff}} = \left[\sqrt{R_2} + \frac{(1-R_2)\sqrt{R_3}}{1+\sqrt{R_2R_3}}\right]^2, \tag{7}$$

where $R_2 = (n_l - n_s)^2/(n_l + n_s)^2$ is the front facet reflectivity of resonant cavity, and $R_3 = (n_s - 1)^2/(n_s + 1)^2$ is the front facet reflectivity of the external cavity.

Considering the Talbot effect, the self-reproducing condition for the jth order supermode oscillation is given by

$$R_1 R_{\mathrm{eff}} \left|C_j\right| \exp\left(2\left(\Gamma g_j - \alpha\right) L_{\mathrm{eff}}\right) = 1, \tag{8}$$

where α is the loss in the composite cavity, L_{eff} is the length of the composite cavity, Γ is the confinement factor, and R_1 is the rear facet reflectivity. The gain threshold of the supermode can be expressed as

$$g_j = \frac{\alpha}{L_{\mathrm{eff}}} + \frac{1}{\Gamma L_{\mathrm{eff}}} \ln\left(\frac{1}{\sqrt{R_1 R_{\mathrm{eff}}\left|C_j\right|}}\right). \tag{9}$$

Figure 3 clearly shows the distributions of the coupling strength and threshold gain of the in-phase and anti-phase modes over a Talbot distance of propagation. The maximum difference in the coupling strength and threshold gain between the in-phase mode and the out-of-phase mode occurs at $Z_t/2$, making it the easiest to realize a highly distinguished mode, and the out-of-phase mode is more likely to lase. The in-phase mode and the out-of-phase mode share the second largest coupling strength difference and threshold gain difference at $Z_t/4$. Fortunately, the in-phase mode has higher coupling strength and lower threshold gain. However, the coupling strength of the in-phase mode at $Z_t/4$ is only half of the out-of-phase mode at $Z_t/2$, since half of the in-phase mode optical field at $Z_t/4$ is horizontally shifted by $p/2$, and the feedback coupling optical field is reflected back to the non-gain region of

the DLA. Therefore, the main function of the designed MDLA is to improve the coupling strength of the in-phase mode by injecting the shifted optical fields of the LRC laser array and SRC laser array into a mutual gain region after the phase compensation. Additionally, in comparison with the initial optical field, the coupling strength becomes lower, while the gain threshold becomes higher after propagating over a Z_t Talbot distance, because of the internal diffraction loss.

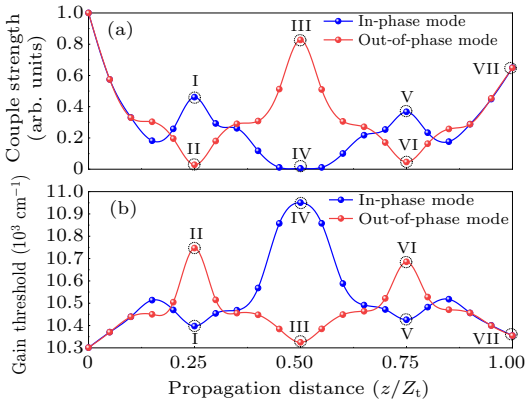


Fig. 3. (a) Coupling strengths and (b) gain thresholds for in-phase mode and out-of-phase mode.

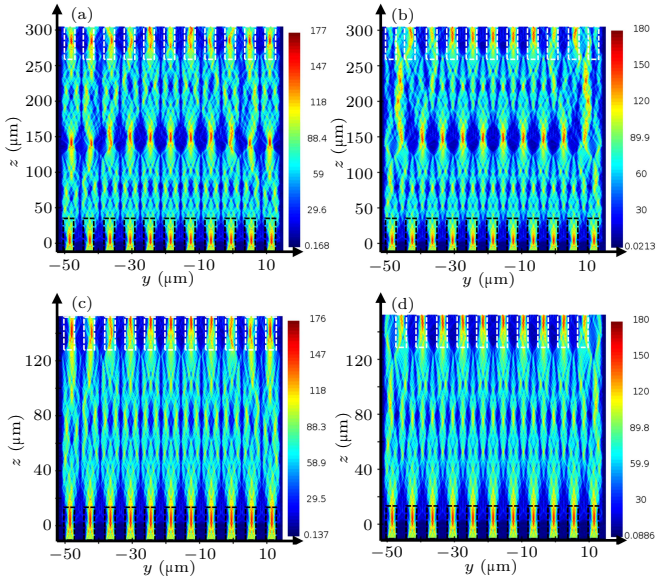


Fig. 4. The Talbot effect in a DLA. Panels (a) and (b) denote the self-imaging of the out-of-phase mode and in-phase mode optical fields at an external cavity length of $Z_t/2$ (propagation distance is Z_t). Panels (c) and (d) denote the self-imaging of the out-of-phase mode optical field and the in-phase mode self-imaging of the optical field is shifted by $p/2$ at an external cavity length of $Z_t/4$ (propagation distance is $Z_t/2$). The black dashed box denotes the initial optical field, while the white dashed box indicates the self-imaging optical field formed subsequent to one round-trip oscillation period of the external cavity.

For DLAs with only one type of resonant cavity, the initial configuration comprised two face-to-face connected $Z_t/2$ external Talbot cavities, which are employed to emulate a round-trip oscillation period (i.e., the propagation distance z is Z_t) in the resonator cavity. Both the out-of-phase and in-phase mode optical fields achieve self-imaging, as demonstrated in Figs. 4(a) and 4(b). This phenomenon signifies that the optical field self-injects back into its own gain region, resulting in the in-phase mode and out-of-phase mode exhibiting comparably high coupling strength and low gain threshold, as shown at "VII" point in Fig. 3. Subsequently, two face-to-face connected $Z_t/4$ external Talbot cavities are constructed to emulate a round-trip oscillation period (i.e., the propagation distance z is $Z_t/2$) in the resonator cavity. As shown in Figs. 4(c) and 4(d), the out-of-phase mode optical field achieves self-imaging, while the in-phase mode self-imaging optical field is shifted by $p/2$, the coupling strength and threshold gain of the two supermodes are shown at "III" and "IV" points in Fig. 3, respectively. It is worth noting that the finite array of units during the simulation leads to boundary effects.

3.2. Self-injection effect of MDLA

It is evident from the preceding analysis that in order to achieve an in-phase mode output, it is necessary to satisfy the condition that the in-phase mode optical field achieves self-injection. The present study has therefore focused on the study of in-phase mode optical field self-injection in the MDLA. The designed MDLA contains 6 LRCs and 5 SRCs; the length difference ΔL between LRC and SRC is 305.06 μm. All resonant cavities are designed with a width w of 3 μm, a period p of 12 μm, and a spacing d of 3 μm. The detailed structural parameters are shown in Table 1.

Table 1. Parameters used in the simulation of MDLA.

Symbol	Parameter	Value
L (μm)	EC_l length for LRC	152.53
$L+\Delta L$ (μm)	EC_s length for SRC	457.59
ΔL (μm)	difference in length between LRC and SRC	305.06
w (μm)	width of ridge waveguide	3
d (μm)	edge-to-edge distance between LRC and SRC	3
p (μm)	period of LRC and SRC	12
h (μm)	height of ridge waveguide	0.74
λ (nm)	wavelength	808
n_s	effective refractive index of external cavity	3.42354
n_l	effective refractive index of resonant cavity	3.42420
Δn	refractive index difference between LRC and SRC cavity length difference region	0.00066

The study commenced with two face-to-face connected $Z_t/8$ external Talbot cavities, which are utilized to emulate a round-trip oscillation period (i.e., the propagation distance is $Z_t/4$) in the resonator cavity. In the case of operating the LRC in the MDLA, the EC_l length L is $Z_t/8$, and the propagation distance $2L$ is $Z_t/4$. Figure 5(a) illustrates that the out-of-phase mode optical field is shifted to the left and to the right by $p/4$ compared to the initial optical field, respectively, and injected into the non-gain region between the neighboring LRC and SRC, resulting in low coupling strength and high

gain threshold, as shown at "II" point in Fig. 3. Figure 5(b) illustrates that the 0-phase optical field in the in-phase mode achieves self-injection, while the one with a $\pi/2$ phase delay is shifted by $p/2$ and injected into the non-gain region between the neighboring LRCs, resulting in half the coupling strength and leading to half the power loss, as shown at "I" point in Fig. 3. It is believed that the essence of the self-imaging of the Talbot optical field is characterised by a multiple of 2π change during propagation. The incorporation of the SRC to establish the MDLA leads to phase modulation of the delayed optical field of the in-phase modes within the LRC and SRC, and the reconstructed in-phase mode optical field within the LRC attains self-injection, as illustrated in Fig. 5(c). At this juncture, the EC_s length $L+\Delta L$ is $3Z_t/8$ for SRC, the propagation distance $2L+2\Delta L$ is $3Z_t/4$, and the in-phase mode self-injection is also achieved, as shown in Fig. 5(d). Furthermore, after increasing the scale of the laser array to 19, the LRC and SRC laser arrays in the MDLA could also realize the in-phase mode self-injection. It can thus be estimated that the self-organized phase-locking of in-phase mode is achieved in the MDLA of larger scale.

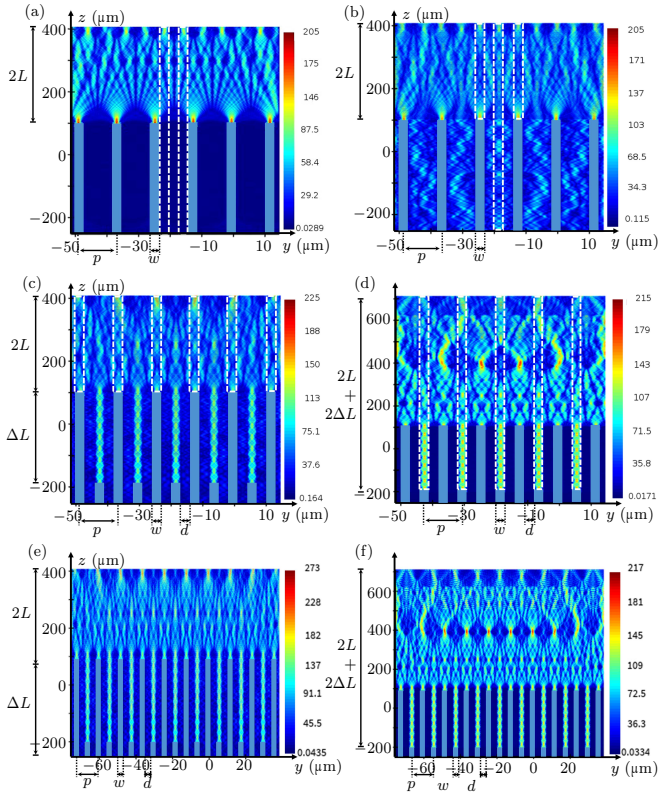


Fig. 5. The Talbot effect in the MDLA. (a) and (b) Laser arrays: in LRC-only operation, the out-of-phase mode is injected into the non-gain region, resulting in complete loss, and there is a half-power loss for the in-phase mode, respectively; (c) and (d) self-injection of the in-phase modes corresponding to both the LRC and the SRC is achieved in the MDLA after the introduction of the SRC; (e) and (f) increasing the scale of the laser array to 19, the LRC and SRC laser arrays in the MDLA could also realize the in-phase mode self-injection. The long and short blue rectangles indicate the LRC and SRC respectively, and the white dashed box represents the round-trip propagating optical field through the external cavity.

3.3. Self-imaging near-field pattern of MDLA

The subsequent analysis focuses on the near-field pattern (NFP) distribution of the MDLA. Figure 6(a) illustrates the NFP of Fig. 5(b) for stable oscillations of the in-phase mode. In scenarios where the LRC functions exclusively in the MDLA, the NFP is characterised by the conventional $Z_t/8$ fractional Talbot optical field distribution. This distribution exhibits five light spots in the NFP, attributable to phase delays. The incorporation of the SRC facilitates the reconstruction of the optical field, resulting in the self-imaging of the in-phase mode optical field, as illustrated in Fig. 5(b). This phenomenon also corresponds to the NFP of the MDLA, which operates stably.

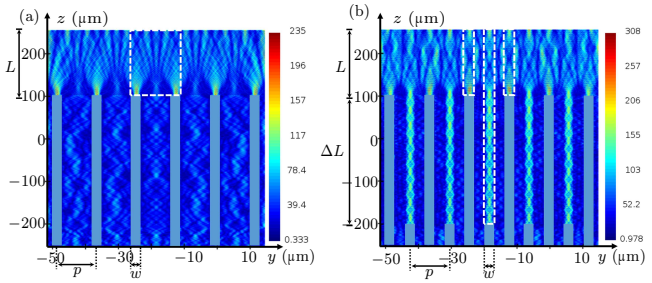


Fig. 6. The NFP of (a) LRC-only operation in the MDLA with five light spots at $Z_t/8$, and (b) MDLA with self-imaging at $Z_t/8$. The white dotted box shows a segment of the output near field when the DLA is operating stably.

3.4. Far-field pattern of MDLA

The FFP of the MDLA was finally analysed, revealing sub-optimal far-field coherence of the in-phase mode of the LCR-only operation in the MDLA due to phase delay. This results in comparatively dispersed optical field energy, with a central peak energy share of only 24.1% and a full width at half maximum (FWHM) of the lateral divergence angle of 4.44°, as illustrated in Fig. 7(a). However, the introduction of SRC-formed MDLA to compensate for the in-phase phase delay enhances the output far-field coherence and the energy is more concentrated in the centre peak with an energy share of 42.3%, which is nearly doubled. Furthermore, the FWHM of lateral divergence angle is reduced to 0.34°, as illustrated in Fig. 7(b). It is important to note that the introduction of SRC leads to an increase in both the number and the fill factor of the DLA. The far-field optical intensity distribution of the DLA is given by

$$I_j(\eta) \propto \left[\frac{\sin\left(N(\eta+\theta)/2\right)}{\sin\left((\eta+\theta)/2\right)} - (-1)^j \frac{\sin\left(N(\eta+\theta)/2\right)}{\sin\left((\eta+\theta)/2\right)}\right]^2 \times \exp\left(-\frac{\delta^2\eta^2}{8}\right), \tag{10}$$

where $I_j(\eta)$ is the far-field optical intensity distribution of the jth order supermode, $j\,(=1,2,\ldots)$ is the jth order supermode, $\eta = kz\sin\theta$ is the parameter controlling phase shift, N is the number of laser units, θ is the divergence angle, and $\delta = w/p$

is the filling factor. As the fill factor becomes smaller, the exponential term modulates the far field more weakly, and the energy of the optical field at the centre of the Gaussian envelope will be more dispersed, whereas as the fill factor becomes larger, the energy of the optical field will be more concentrated near the center.[31]

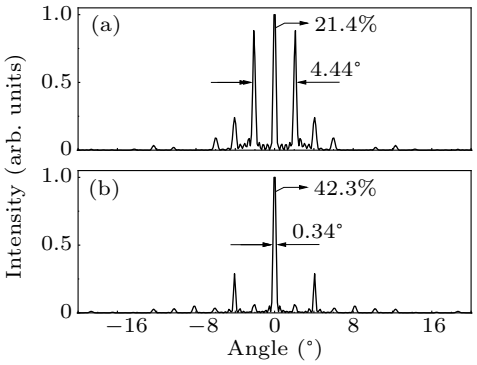


Fig. 7. The FFP of (a) the LCR-only operation in the MDLA with an underdetermined in-phase mode and (b) MDLA with an excellent coherence in-phase mode.

4. Conclusion

In conclusion, we propose a self-organized phase-locking MDLA with on-chip Talbot effect and analyze the mechanism of the dual Talbot diffraction coupling process. Through the rational design of the LRC, SRC, and external Talbot cavity, the NFP distributions of the MDLA can be reconfigured to form self-imaging as expected, and the efficient mutual injection of the in-phase mode optical field between LRC and SRC can effectively reduce the optical loss. Additionally, the compensation of the in-phase mode phase delay caused by the fractional Talbot effect has been demonstrated to enhance the coherence of the in-phase mode of the MDLA. As a result, the central peak energy is increased from 21.4% to 44.3%, while the FWHM of the lateral divergence angle is reduced from 4.52° to 0.34°, which significantly improves the quality of the laser beam. Finally, the proposed dual Talbot diffraction coupling method could be beneficial for achieving high-power and high-beam-quality lasers.

Acknowledgement

This research was funded by the Science and Technology Commission Foundation of the Central Military Commission (Grant No. 2023-JCJQ-JJ-1008).

References

[1] Zhang Y S, Xu Y F, Zheng J L, Li L Y, Fang T and Chen X F 2023 *Chin. Phys. B* **32** 094204
[2] Gen P F, Chen M, An X Y, Liu W Y, Zhu X Z, Li J L, Li B Y and Sheng Z M 2023 *Chin. Phys. B* **32** 044101
[3] Zhang G B, Liu S, Zou D B, Cui Y, Liu J P, Yang X H, Ma Y Y and Shao F Q 2023 *Chin. Phys. B* **32** 095202
[4] Etemadi A, Khajehmougahi K, Solimei L, Benedicenti S and Chiniforush N 2024 *Appl. Sci.* **14** 847
[5] Xu H, Li Z Q, Pang C, Li R, Li G L, Akhmadaliev S, Zhou S Q, Lu Q M, Jia Y C and Chen F 2022 *Chin. Phys. B* **31** 094209
[6] Bai W C, Qin W Z, Tang D, Ji F M, Chen H S, Yang F, Qiao Z Q, Duan T, Lin D, He R, Zhu W K and Wang L 2021 *Opt. Laser Technol.* **139** 106989
[7] Zhang W Q, Liu W Z, Wang J W, Cao P, Chen J X, Ting F, Zhou X Y and Zheng W H 2022 *Opt. Lett.* **47** 5012
[8] Adams M, Holly C, Rauch S, Traub M, Hoffmann H and Haefner C 2024 *Opt. Express* **32** 6446
[9] Evered C, Li K and Fan Y L 2024 *Opt. Lett.* **49** 3524
[10] Yuan M Y, Wang W Q, Wang X Y, Wang Y, Yang Q H, Cheng D, Liu Y, Huang L, Zhang M R, Liang B, Zhao W and Zhang W F 2021 *Opt. Lett.* **46** 4855
[11] Chang G L, Zhu H, Yu C R, Zhu H Q, Xu G Y and He L 2020 *Infrared Phys. Technol.* **109** 103427
[12] Ackley D E 1983 *Appl. Phys. Lett.* **42** 452
[13] Botez D, Hayashida P, Mawst L J and Roth T J 1988 *Appl. Phys. Lett.* **53** 1366
[14] Naurois G M, Carras M, Simozrag B, Patard O, Alexandre F and Marcadet X 2011 *AIP Adv.* **1** 032165
[15] Liu Y H, Zhang J C, Yan F L, Liu F Q, Zhuo N, Wang L J, Liu J Q and Wang Z G 2015 *Appl. Phys. Lett.* **106** 142104
[16] Jiang W and Chakraborty S 2021 *Opt. Lett.* **46** 1137
[17] Wenzel H, Crump P, Fricke J, Ressel P and Erbert G 2013 *IEEE J. Quantum Electron.* 491102
[18] Lyakh A, Maulini R, Tsekoun A, Go R and Patel C K N 2014 *Opt. Express* **22** 1203
[19] Kirch J D, Chang C C, Boyle C, Mawst L J, Lindberg D, Earles T and Botez D 2015 *Appl. Phys. Lett.* **106** 061113
[20] Kao T Y, Hu Q and Reno J L 2010 *Appl. Phys. Lett.* **96** 101106
[21] Zhou X Y, Qu H W, Qi A Y, Ma X L, Zhao S Y, Wang Y F and Zheng W H 2018 *IEEE Photonics Technol. Lett.* **30** 1645
[22] Jia Z W, Wang L, Zhang J C, Zhao Y, Liu C W, Zhai S Q, Zhuo N, Liu J Q, Wang L J, Liu S M, Liu F Q and Wang Z G 2017 *Appl. Phys. Lett.* **111** 061108
[23] Xu Y F, Sun Y Q, Li W J, Ma Y, Zhuo N, Liu J Q, Zhang J C, Zhai S Q, Liu S, Wang L J and Liu F Q 2022 *Opt. Express* **30** 36783
[24] Zhao Y, Zhang J C, Cheng F M, Wang D B, Liu C W, Zhuo N, Zhai S Q, Wang L J, Liu J Q, Liu S, Liu F Q and Wang Z G 2018 *Nanoscale Res. Lett.* **13** 205
[25] Qi J, Lan T, Ma W, Zhang J, Li Y, Li D Z, Liu X S and Wang Z Y 2024 *Opt. Laser Technol.* **177** 111168
[26] Leger J R 1989 *Appl. Phys. Lett.* **55** 334
[27] Zhou C and Liu L 1995 *Opt. Commun.* **1** 115
[28] Wen C Y, Li W, Dai J J, Ma S F and Wang Z Y 2023 *Photonics* **10** 115
[29] Lei W, Dai J J, Li S N, Jin D Y and Wang Z Y 2024 *J. Lightwave Technol.* **42** 8263
[30] Wang X F, Xu N, Gong Y H and Li J W 2025 *Infrared Laser Eng.* **54** 20240448
[31] Pan G Z, Xun M, Sun Y, Zhao Z Z, Xu C, Xie Y Y, Wu D X and Zhou J T 2022 *Opt. Laser Technol.* **149** 107809